


A comparative study of epitaxial InGaAsBi/InP structures using Rutherford backscattering spectrometry, X-ray diffraction and photoluminescence techniques

Cite as: J. Appl. Phys. **126**, 125706 (2019); <https://doi.org/10.1063/1.5109653>

Submitted: 14 May 2019 . Accepted: 05 September 2019 . Published Online: 26 September 2019

M. K. Sharpe , I. P. Marko , D. A. Duffy , J. England , E. Schneider, M. Kesaria , V. Fedorov, E. Clarke , C. H. Tan , and S. J. Sweeney 

COLLECTIONS

Paper published as part of the special topic on [Highly Mismatched Semiconductors Alloys: from Atoms to Devices](#)

Note: This paper is part of the Special Topic on Highly Mismatched Semiconductors Alloys: From Atoms to Devices.



View Online



Export Citation



CrossMark

ARTICLES YOU MAY BE INTERESTED IN

[Scaled experiments on cavity confined explosions in limestone and poly\(methyl methacrylate\)](#)

Journal of Applied Physics **126**, 125901 (2019); <https://doi.org/10.1063/1.5109376>

[Role of intrinsic and extrinsic defects in H implanted hydrothermally grown ZnO](#)

Journal of Applied Physics **126**, 125707 (2019); <https://doi.org/10.1063/1.5115597>

[Terahertz field confinement and enhancement in various sub-wavelength structures](#)

Journal of Applied Physics **126**, 120901 (2019); <https://doi.org/10.1063/1.5110046>

Lock-in Amplifiers up to 600 MHz

starting at

\$6,210



 Zurich
Instruments

Watch the Video



A comparative study of epitaxial InGaAsBi/InP structures using Rutherford backscattering spectrometry, X-ray diffraction and photoluminescence techniques

Cite as: J. Appl. Phys. 126, 125706 (2019); doi: 10.1063/1.5109653

Submitted: 14 May 2019 · Accepted: 5 September 2019 ·

Published Online: 26 September 2019



View Online



Export Citation



CrossMark

M. K. Sharpe,¹ I. P. Marko,² D. A. Duffy,² J. England,¹ E. Schneider,^{1,2} M. Kesaria,^{3,b)} V. Fedorov,^{3,4} E. Clarke,³ C. H. Tan,³ and S. J. Sweeney^{2,a)}

AFFILIATIONS

¹Advanced Technology Institute, Ion Beam Centre, University of Surrey, Guildford GU2 7XH, United Kingdom

²Advanced Technology Institute and Department of Physics, University of Surrey, Guildford GU2 7XH, United Kingdom

³Department of Electronic and Electrical Engineering, University of Sheffield, Sheffield S1 4DE, United Kingdom

⁴Saint Petersburg Academic University, St. Petersburg 194021, Russia

Note: This paper is part of the Special Topic on Highly Mismatched Semiconductors Alloys: From Atoms to Devices.

^{a)}**Author to whom correspondence should be addressed:** s.sweeney@surrey.ac.uk

^{b)}**Present address:** Department of Physics and Astronomy, Cardiff University, Cardiff CF24 3AA, United Kingdom.

ABSTRACT

In this work, we used a combination of photoluminescence (PL), high resolution X-ray diffraction (XRD), and Rutherford backscattering spectrometry (RBS) techniques to investigate material quality and structural properties of MBE-grown InGaAsBi samples (with and without an InGaAs cap layer) with targeted bismuth composition in the 3%–4% range. XRD data showed that the InGaAsBi layers are more homogeneous in the uncapped samples. For the capped samples, the growth of the InGaAs capped layer at higher temperature affects the quality of the InGaAsBi layer and bismuth distribution in the growth direction. Low-temperature PL exhibited multiple emission peaks; the peak energies, widths, and relative intensities were used for comparative analysis of the data in line with the XRD and RBS results. RBS data at a random orientation together with channeled measurements allowed both an estimation of the bismuth composition and analysis of the structural properties. The RBS channeling showed evidence of higher strain due to possible antisite defects in the capped samples grown at a higher temperature. It is also suggested that the growth of the capped layer at high temperature causes deterioration of the bismuth-layer quality. The RBS analysis demonstrated evidence of a reduction of homogeneity of uncapped InGaAsBi layers with increasing bismuth concentration. The uncapped higher bismuth concentration sample showed less defined channeling dips suggesting poorer crystal quality and clustering of bismuth on the sample surface.

Published under license by AIP Publishing. <https://doi.org/10.1063/1.5109653>

INTRODUCTION

Adding bismuth into conventional III-V semiconductors gives rise to a large bandgap reduction. Substituting arsenic atoms in conventional III-V compounds and alloys with small amounts of bismuth creates an energy state in the host valence band (VB), which interacts with the host valence band states. This causes a valence band anticrossing (VBAC) interaction.¹ This strongly reduces

the bandgap, E_g , by ~ 80 meV/Bi% and ~ 56 meV/Bi% in GaAsBi and InGaAsBi, respectively,^{2–6} and hence opens up possibilities to extend the spectral range of GaAs- and InP-based light emitting and detecting devices into the mid-infrared.^{4,6} At the same time, incorporating bismuth strongly increases the spin-orbit splitting energy separation, Δ_{SO} . This is due to both the effects of an enhanced electron spin-orbital (SO) angular momentum interaction within the heavy

bismuth atoms and the upward movement of the valence band maximum. For bismuth compositions for which $\Delta_{\text{SO}} > E_g$, the deleterious effects of processes such as Auger recombination (involving excitation of a hot hole into the spin-orbit split off band; the so-called CHSH process) and intervalence band absorption (IVBA) can be suppressed. These processes limit the performance and efficiency of the near- and mid-infrared photonic devices. Figure 1 presents a summary of experimental data of the compositional dependence of E_g and Δ_{SO} in GaAsBi and InGaAsBi with a fixed indium fraction of 53% as a function of bismuth concentration, which is in good agreement with theoretical VBAC calculations presented in the figure.^{3,4,6} From these data, it is shown that the energy crossover ($\Delta_{\text{SO}} > E_g$) occurs at bismuth concentrations around 10% in GaAsBi^{3,4,7} and at 3%–4% bismuth in the InGaAsBi alloy system on InP.^{5,6} Such alloys, therefore, offer a practical route to reduce, or even eliminate, fundamental loss processes such as Auger recombination and IVBA, which is expected to significantly improve the temperature stability of device output power, with the added benefit of growth on well-established GaAs and InP substrates using well-established III-V device fabrication technologies. GaAsBi/GaAs is suitable for the near-IR, particularly, 1.55 μm telecom devices, while InGaAsBi could span a wide spectral range from the near- and mid-IR out to $>6 \mu\text{m}$, while still maintaining tolerable strain levels on standard InP substrates. In addition, for detector applications 3.2% Bi incorporation leads to a cutoff wavelength of about 2.1 μm at room temperature.⁸ The application of mid-infrared devices on InP is particularly promising owing to the fact that (i) a much smaller fraction of bismuth is required to achieve the preferential band structure compared to indium, (ii) InGaAsBi/InP heterostructures can exploit well-established conventional InP telecoms device processing, and (iii) the fact that InP substrates are much cheaper and more

thermally conductive than GaSb as conventionally used for interband mid-infrared devices.

Despite the inspiring potential of III-V-bismide alloys, there are several main challenges related to practical realization of bismuth containing photonic devices. These are related to growth issues and difficulty in incorporating large bismuth atoms into the III-V crystal lattice. This requires a reduced growth temperature and consequently leads to a deterioration of the material quality. Wang *et al.* presented a comprehensive review discussing the historical development of epitaxial growth methods of different bismide alloys, discussing in detail most of the challenges and progress in material growth.⁹ During the past decade, most of the focus has been on developing near-infrared bandgap GaAsBi based structures on GaAs substrates. This has resulted in the demonstration of electrically pumped quantum well (QW) lasers with bismuth compositions of up to 6% and maximum room temperature lasing wavelengths of 1142 nm.^{10–12} The threshold current densities of these devices are relatively high compared to the bismuth-free material, which has been shown to be due to defect-related recombination.^{11,13} The main limiting factors affecting the devices are nonradiative recombination via defects and inhomogeneity effects caused by low-temperature growth and difficulties of bismuth incorporation.¹⁴ Therefore, understanding and optimization of growth methods for production of high optical quality semiconductor structures remains one of the main tasks for practical deployment of III-V-bismide alloys in device applications.

In this paper, we use photoluminescence (PL) and Rutherford backscattering spectrometry (RBS) techniques in combination with high resolution X-ray diffraction (XRD) for structural characterization of InGaAsBi/InP-based epitaxial structures to understand the effects of growth conditions on bismuth incorporation, crystallographic structures, and the optical properties of InGaAsBi/InP-based alloys for mid-infrared applications.

InGaAsBi samples and preliminary characterization using XRD and photoluminescence

A series of four samples were grown using molecular beam epitaxy (MBE) on 2 in. sulfur-doped n-InP wafers using a VG V80 MBE system. Following oxide removal, a 200 nm undoped and nominally lattice-matched $\text{In}_{0.53}\text{Ga}_{0.47}\text{As}$ buffer layer was grown with a growth rate of 0.63 ML/s at a substrate temperature of 500 °C and an As_2 beam equivalent pressure (BEP) of 8×10^{-6} mbar (As_2 :III ratio of 21:1), with an indium flux of 2.1×10^{-7} mbar and a gallium flux of 1.7×10^{-7} mbar. The temperature was then lowered for deposition of a 100 nm InGaAsBi layer, at the temperatures specified in Table I. Prior to the growth of the InGaAsBi layer, the surface was exposed to a bismuth flux for 30 s to soak the surface with bismuth, which was intended to increase bismuth incorporation as previously demonstrated for GaAsBi growth.^{15,16} The InGaAsBi layer was grown using the same indium and gallium fluxes as used for the buffer layer, with a reduced As_2 BEP of $(3.0 \pm 0.1) \times 10^{-6}$ mbar (As_2 :III ratio of 7.9:1) for all samples to allow bismuth incorporation into the layer while avoiding arsenic deficiency during growth (which would lead to a poor surface morphology). The bismuth BEP was intentionally varied between 3.7×10^{-8} mbar and 1.2×10^{-7} mbar with all other

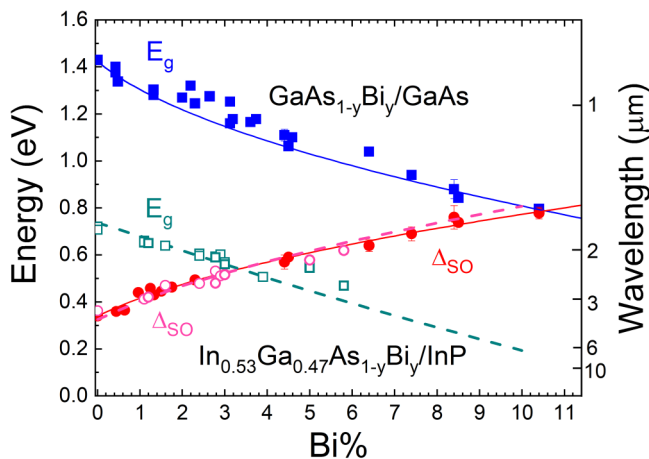


FIG. 1. The room temperature bandgap energy (E_g) and spin-orbit splitting energy (Δ_{SO}) for unstrained $\text{GaAs}_{1-y}\text{Bi}_y/\text{GaAs}$ and $\text{In}_{0.53}\text{Ga}_{0.47}\text{As}_{1-y}\text{Bi}_y/\text{InP}$. The solid and dashed curves represent VBAC theoretical calculations for the case of GaAsBi and InGaAsBi, respectively. The data points show the experimental results (full symbols—GaAsBi/GaAs, open symbols—InGaAsBi/InP) of different authors discussed in detail elsewhere.^{3–6}

TABLE I. MBE-grown InGaAsBi/InP deposition temperatures and bismuth fluxes for each sample investigated in this work.

Sample name	Capped or uncapped	200 nm InGaAs buffer T_{Growth} (°C)	100 nm InGaAsBi T_{Growth} (°C)	InGaAsBi bismuth flux (mbar)	100 nm InGaAs cap T_{Growth} (°C)
C1	InGaAs cap layer	500	370	1.21×10^{-7}	20 nm at 370, then 80 nm at 500
C2	InGaAs cap layer	500	310	1.13×10^{-7}	20 nm at 310, then 80 nm at 500
UC1	Uncapped	500	310	3.72×10^{-8}	
UC2	Uncapped	500	310	5.5×10^{-8}	

element fluxes kept constant for these samples, resulting in layers of different bismuth compositions. For the samples C1 and C2, the InGaAsBi layer was capped by a 100 nm InGaAs layer grown under nominally the same conditions as the buffer layer, except that the first 20 nm was grown immediately following the InGaAsBi layer at the same substrate temperature, then the temperature was increased to 500 °C for the subsequent growth of the remaining 80 nm InGaAs. For samples UC1 and UC2, growth was terminated at the end of the InGaAsBi layer.

After growth, the samples were characterized using high resolution XRD, with ω -2 θ measurements of the (004) reflection obtained using a Bruker D8 Discover X-ray diffractometer. Figure 2 shows the XRD patterns for both capped C1 and C2 samples and uncapped UC1 and UC2 samples, along with simulated fits (calculated using the commercial software package X'Pert Epitaxy with lattice constants for GaBi and InBi of 6.324 Å and 6.686 Å, respectively¹⁷) assuming ideal and homogeneous layers with abrupt interfaces. For each sample, the highest intensity peak at 0° corresponds to the InP substrate. To the left of the substrate peak, a lower angle peak corresponding to the InGaAsBi layer can be

observed (except in the case of C1), demonstrating some evidence of bismuth incorporation into the InGaAs host lattice. This results in a lower angle diffraction peak compared to lattice-matched InGaAs due to the increase in lattice constant with substitutional bismuth incorporation. The more distinct Pendellösung fringes around the quaternary layer in the uncapped samples qualitatively suggest a more uniform layer with sharper interfaces than the capped samples, with the degradation in peak intensity and Pendellösung fringe extrema compared to ideal simulations indicating a reduced crystalline quality and/or the presence of interface roughness, respectively.

The capped sample C1 showed no clear peak indicating evidence of bismuth incorporation when modeled using a single uniform layer despite the presence of bismuth flux during the growth, which was attributed to a higher temperature of 370 °C compared to 310 °C used for the other samples. For the other capped sample (C2), a broad InGaAsBi peak with attenuated Pendellösung fringes potentially indicates some level of relaxation and/or inhomogeneity (an uneven distribution of bismuth) in the InGaAsBi layer.² This could be caused by an uneven distribution of bismuth in the InGaAsBi layer, as shown previously for GaAsBi by Reyes *et al.*¹⁸

In addition to the InGaAsBi peak, in the case of C1, C2, and UC1, a higher angle peak is observed to the right of the substrate. This is attributed to a slight lattice mismatch in the InGaAs cap and/or buffer layer(s) under tensile strain, indicating insufficient indium incorporation during growth.

In the quaternary InGaAsBi alloy, both indium and bismuth atoms cause an increase in the lattice constant; hence, the exact composition of bismuth cannot be determined unambiguously from a single conventional (004) XRD measurement alone. In Fig. 2, approximate bismuth fractions were obtained from fitting dynamical diffraction models to the experimental diffraction patterns while assuming fully pseudomorphically strained layers with a fixed indium fraction of 53%. The XRD simulations appear to reproduce the general features of the uncapped samples. However, in the case of the capped samples with less defined broad bismuth features poorer fits were obtained for an ideal multilayer model, which we attribute to the previously speculated inhomogeneity and possible relaxation in the quaternary layer. As additional techniques to characterize the composition of InGaAsBi layers and their quality, we used photoluminescence and RBS measurements. The results of different techniques and their consistency with each other will be presented and discussed further in this paper.

For optical characterization of the samples, we used a photoluminescence setup including a ThermoFisher iS50 FTIR spectrometer, a liquid nitrogen cooled InSb detector, a continuous

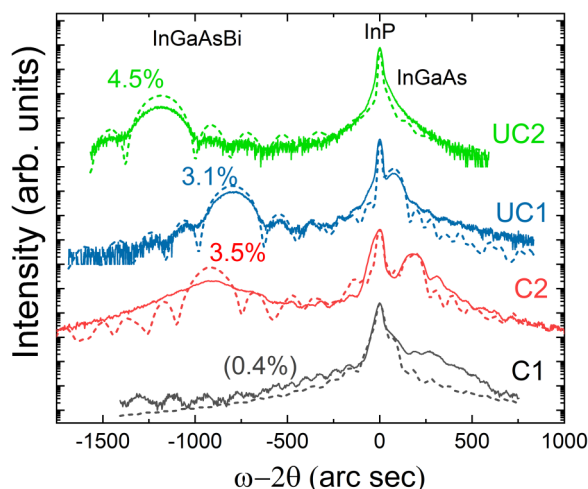


FIG. 2. XRD scans for the InGaAsBi samples including two uncapped samples UC1 and UC2 and two InGaAs cap layer samples C1 and C2, offset for clarity. Approximate bismuth fractions for each sample are included for fixed indium fractions of 53%, with C1 being poorly reproduced from XRD modeling of a single uniform layer.

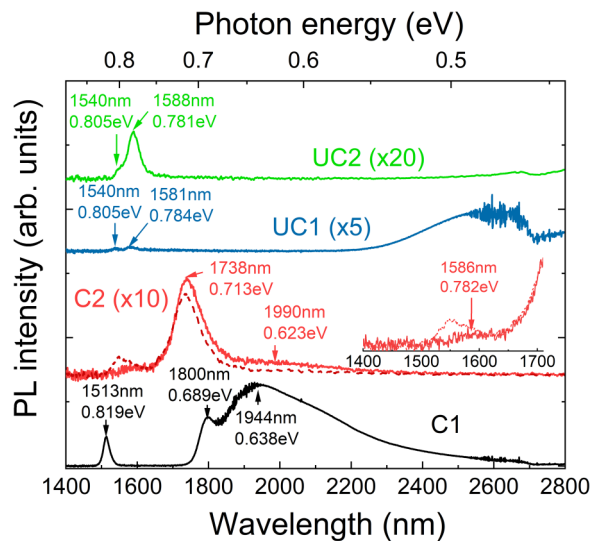


FIG. 3. PL spectra of InGaAsBi samples studied in this work measured at 15 K and continuous wave 532 nm laser excitation at 950 mW. The dashed line is the PL spectrum measured from the sample C2 from another position on the wafer closer to its growth edge (the other samples did not show a significant variation of PL across the wafer). The spectra for C2, UC1, and UC2 are scaled with the scaling factor given near the corresponding sample labels. The insert shows weak PL peaks in sample C2 in more detail.

wave (CW) 532 nm DPSS Laser Quantum Opus laser, and a closed cycle He-refrigerator cryostat controlling sample temperature in the range of 10–300 K.

None of the samples showed PL signal at room temperature in the setup used. Figure 3 presents the PL spectra of all four samples at 15 K under an excitation laser power of 950 mW, with a spot size of 1.85 mm. The PL spectra consisted of multiple peaks, as summarized in Table II. There are various potential reasons for the multitude of peaks caused by compositional inhomogeneity in both in-plane and growth directions of the InGaAsBi layer, possibly the presence of localized states and defect-related traps discussed below. The spectra were corrected using the system response function but were affected by noise due to strong water absorption in the air over the spectral ranges of 1800–1950 nm (0.635–0.689 eV) and 2530–2800 nm (0.443–0.490 eV). To estimate the bismuth relation corresponding to each PL peak, we used the peak shift, ΔE_g , relative to the bandgap of $\text{In}_{0.53}\text{Ga}_{0.47}\text{As}$. This was calculated by subtracting the photon energy of the PL peak from the photon energy peak corresponding to the InGaAs cap or buffer layer. Using the value of ΔE_g and the E_g curve for InGaAsBi in Fig. 1, the corresponding bismuth composition was estimated for each PL peak. Uncertainty of 10–15 meV in the PL peak position would cause an error of 0.2% bismuth as estimated from Fig. 1. The cap/buffer layer PL was the strongest in sample C1 and as much as 50 or more times weaker in the other samples. The maximum temperature, above which the PL signal became undetectable, is also given in Table II for comparison of the samples. Capped sample C1 demonstrated the strongest, but the broadest, PL signal with the presence of longer

TABLE II. PL peak positions obtained from the spectra presented in Fig. 1. The peak shifts, ΔE_g , were calculated by subtracting the photon energies of the PL peak corresponding to the $\text{In}_{0.53}\text{Ga}_{0.47}\text{As}$ cap or buffer layer from the photon energies of each peak. Using the value of ΔE_g and E_g curve for InGaAsBi in Fig. 1, a possible bismuth composition was estimated assuming the nominal indium fraction.

Sample	Maximum T (K)	PL peak/emission band (eV)	ΔE_g (meV)	Bi %
C1	160	0.819	0	0
		0.689	130	2.2
		0.638	181	3.07
C2 ^a	80	0.47–0.63	189–349	3.22–6.1
		0.782	37	0.66
		0.713	106	1.8
		0.623	196	3.4
UC1	30	0.805	0	0
		0.784	21	0.38
UC2	15	0.47–0.55	255–335	4.4–5.86
		0.805	0	0
		0.781	24	0.4
		0.462	343	6.0

^aInGaAs buffer/cap layers peak in sample C2 was very weak and poorly defined being close to the position of the well-defined corresponding InGaAs peak in sample C1 (0.819 eV), which was used to estimate the ΔE_g values in sample C2.

wavelength peaks compared with the bandgap of $\text{In}_{0.53}\text{Ga}_{0.47}\text{As}$ as shown in Table II, which may indicate incorporation of bismuth as shown in the table. However, given that there was little evidence of bismuth incorporation from XRD, the origin of the long-wavelength emission is uncertain in this sample. It may be caused by various reasons, including possible localized states with strong PL signal at longer wavelengths at low temperature⁵ and/or recombination via defect-related traps¹⁹ caused by the low growth temperature. We make a note of caution here that such long-wavelength emission bands may also relate to the low-temperature grown InGaAs layer of the cap as we recently observed in InGaAs p-i-n structures grown at 350 °C demonstrating a weak PL emission in the range of 0.4–0.7 eV, which is a focus of further investigations. The formation of bismuth nanocrystals was previously observed in GaAsBi/AlAs superlattices, giving rise to strong PL signals with wavelengths ranging from 1.3 to 1.7 μm after postgrowth annealing.²⁰ It should be noted that the PL signal was independent of position on the wafer in samples C1, UC1, and UC2 with a small relative variation of intensities of different peaks in the sample C2. For sample C2, the dashed curve in Fig. 3 shows the PL measured away from the wafer center, whereas the solid lines were obtained from the central part of the wafers, showing evidence of some spatial nonuniformity; this was not observed in the other samples. The resulting values for bismuth compositions estimated from the PL peaks will be discussed later in this paper in comparison with the results of XRD and RBS analysis.

Rutherford backscattering measurements

XRD and PL characterization techniques are unable to give a complete picture regarding the composition of elements in the

InGaAsBi quaternary alloy because both indium and bismuth give rise to a reduced bandgap as well as causing an increase in lattice constant, and strain if unrelaxed.⁶ To extend the material characterization, we used Rutherford backscattering spectrometry (RBS) to more accurately analyze the bismuth content of the InGaAsBi layers and, using channeling measurements, to investigate the crystallographic quality and nature of the defects. The RBS experimental setup used in this work is described in detail elsewhere.²¹ Briefly, the technique involved directing a collimated beam of helium ions onto the samples and measuring the number and energy of ions scattered into particular directions using particle detectors. The results reported in this paper measured ions scattered through an angle of 148.6° (Ref. 22) in an “IBM geometry,” where the incident beam, detector position, and surface normal were in the same plane. Mounting the sample on a goniometer²¹ allowed channeling RBS measurements to be carried out. For random RBS measurements, the goniometer was first aligned so that the beam was directed along the (001) direction of the sample and then rotated by 2° around both the horizontal and vertical axes.

The major energy loss of the primary ions arises from the kinematic factors of their collisions with the sample atoms. The number and energy of scattered ions increases with the mass of the scattering atom. The ions lose further energy through electronic stopping along their inward (precollision) paths and then along their outward (postcollision) paths. The final energy of an ion characterizes the mass and depth of the scattering atom from which it was scattered.

Bismuth has a significantly larger atomic mass compared to indium, gallium, and arsenic, and so ions scattered from bismuth atoms had the highest energies. The helium ion beam energy, chosen to be 4 MeV, allowed the bismuth peak to occur over energies in the RBS spectrum at higher channels than for any signals from other more abundant elements in the sample. This allowed the relatively small number of counts in the peak to be unambiguously assigned to bismuth, without the need to remove significant contributions from other elements. This was possible in both the uncapped (with bismuth in the surface layer) and capped samples (with bismuth in a buried layer). The sensitivity for bismuth was also good because its large mass gave a large RBS cross section and hence relatively high number of scattering events per atom. Previous RBS studies on InGaAsBi by Feng *et al.*²³ had used lower ion energies

(around 2 MeV) so that the bismuth peak overlapped with the other elements making it harder to unambiguously identify. To demonstrate this effect, Figs. 4(a) and 4(b) show the randomly oriented RBS spectra for different ion beam energies of 2 MeV and 4 MeV, respectively, simulated for the $\text{In}_{0.53}\text{Ga}_{0.47}\text{As}/\text{In}_y\text{Ga}_{1-y}\text{As}_{1-x}\text{Bi}_x/\text{In}_{0.53}\text{Ga}_{0.47}\text{As}/\text{InP}$ structure as well as the RBS experimental spectra measured in this work [see Fig. 4(b)]. It should be noted that the gallium and arsenic atomic masses are similar and hence their RBS peaks overlap. While the signal from indium near the surface is at higher energies than the gallium and arsenic peaks, the presence of indium in all layers, including the substrate, means that the signal from this element dominates the spectrum.

The bismuth peak is clearly differentiated in the 4 MeV beam energy data illustrating the importance of operating at higher beam energies. 4 MeV is also a good compromise for bismuth peak separation while still having adequate depth resolution, whereas higher beam energies would further reduce the depth resolution. We also note that this beam energy and intensity did not show any evidence of damage creation in the crystals. The time spent collecting each spectrum was chosen so that the sample was bombarded with 5 μC of helium ions. This charge was a compromise between the collection of sufficient data for improved counting statistics vs causing damage to the sample. After continuous exposure, no difference was observed in the quality of the thin film channeling measurements, indicating minimal damage to the sample epilayers throughout the total set of measurements for this beam energy and charge.

The elemental compositions for each layer of the samples were calculated after simulating the measured random (nonchanneled) RBS spectra using the SIMNRA program.²⁴ With the bismuth feature being fully separated from the other elements, bismuth compositions for the quaternary InGaAsBi layers were obtained with measurement uncertainties of 5% (relative), dominated by counting statistics. Table III compares the compositions for indium and bismuth obtained via RBS to the predictions from the XRD and PL data presented earlier in this paper. The RBS data indicate a bismuth fraction of $\sim 1.2\%$ in the capped sample C1, despite the absence of Bi-related feature in the XRD spectrum (see Fig. 2). This sample exhibited very strong broad low-temperature PL in the spectral range 1750–2800 nm, which indicated the presence of localized states. We cannot rule out the possibility of recombination via defect-related traps either in InGaAsBi layer itself¹⁹ or the

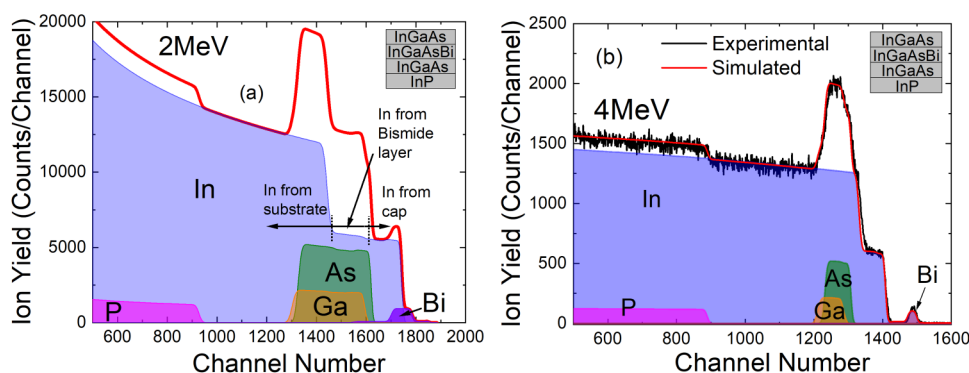


FIG. 4. Comparison of RBS spectra for (a) 2 MeV and (b) 4 MeV ion beam energies on an InGaAs capped InGaAsBi sample. Contributions from P, Ga, As, In, and Bi are based on simulations, with (b) including the experimental RBS spectra. The bismuth peak is more distinct when using 4 MeV ion beam energies.

TABLE III. Elemental percentages obtained from the random RBS for the $\text{In}_x\text{Ga}_{1-x}\text{As}_{1-y}\text{Bi}_y$ samples. XRD and PL predicted percentages included. The bismuth fractions deduced from the PL results correspond to the PL peaks as given in Table II.

Sample	XRD		PL		RBS	
	In (%)	Bi (%)	In (%)	Bi (%)	In (%)	Bi (%)
C1	53	0.4% (ambiguous)	53	0 2.2 3.07 3.22–6.1	52	1.2
C2	53	3.5	53	0.66 1.8 3.4	53	3.2
UC1	53	3.1	53	0 0.38 5.5–5.86	53	2.1
UC2	53	4.5	53	0 0.4 6.0	53	3.2

low-temperature grown part of the InGaAs cap layer, but usually such emission would have relatively weak intensity due to the longer lifetime of trapped carriers. The other capped sample, C2, grown at a lower temperature, showed weaker PL compared to C1 with significantly reduced long-wavelength emission beyond 1900 nm and demonstrated a better agreement in bismuth composition obtained from PL (1.8% and 3.4% Bi for the main peak at 0.713 eV and weaker broad emission around 0.623 eV, respectively), XRD (3.5% Bi), and RBS (3.2% Bi). The PL signals in the uncapped samples were very weak and detectable only at low temperatures below 30 K, which indicates relatively poor material quality and, consequently, very low PL efficiency. The bismuth compositions implied by the variation of InGaAsBi bandgaps with bismuth compositions (assuming an indium composition of 53%) are different from the ones obtained from XRD and RBS and suggest that the origin of the PL may relate to localized states.

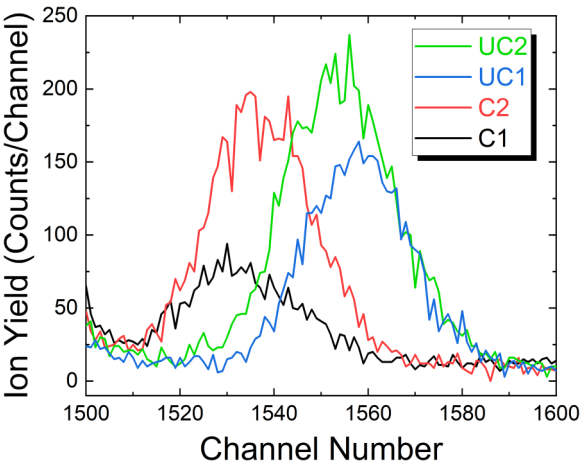


FIG. 5. Comparison of the bismuth peak in the random angle RBS curves for all InGaAsBi samples. Asymmetry in the bismuth peak may suggest an uneven bismuth distribution in the layer.

The variation in results may be due to inhomogeneity in bismuth concentration in the layers and the presence of nonsubstitutional bismuth. Among the reasons causing the relatively higher intensity of the PL spectra from the capped samples C1 and C2 could be the improved quality of the InGaAsBi layer due to annealing effects during the higher temperature cap deposition (that, however, may not always be the case if the growth conditions for capped and uncapped samples are different) and/or improved carrier confinement in the InGaAsBi layer due to the wider bandgap InGaAs cap layer. Figure 5 shows the bismuth peaks of the random RBS spectra for all the samples so that the bismuth distributions in the InGaAsBi layers can be compared.

The use of 4 MeV as the primary beam energy separates out the bismuth from the other elements in the RBS spectra but degrades the depth resolution of the measurements (because electronic stopping reduces as primary energy is increased). It is not,

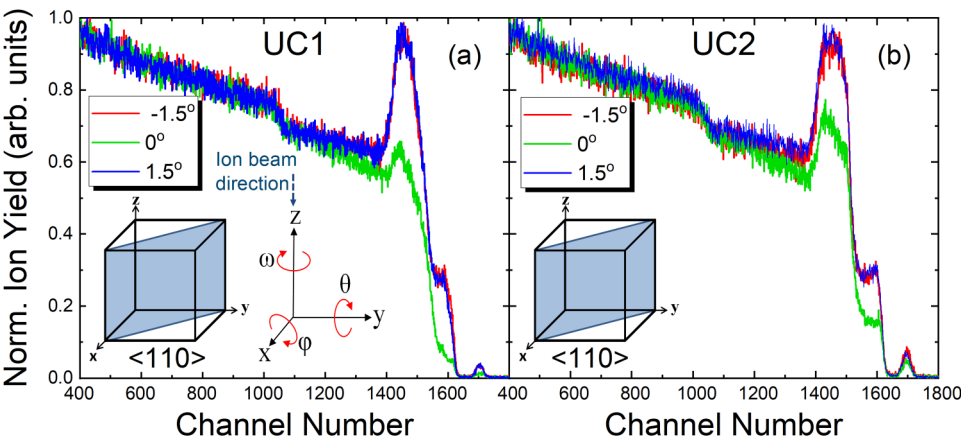


FIG. 6. Comparison of the channeling RBS spectra for (a) sample UC1 and (b) sample UC2. The aligned direction is for the $\langle 110 \rangle$ and the random is for a tilt of 1.5° and -1.5° either side of the same channel along a fixed axis.

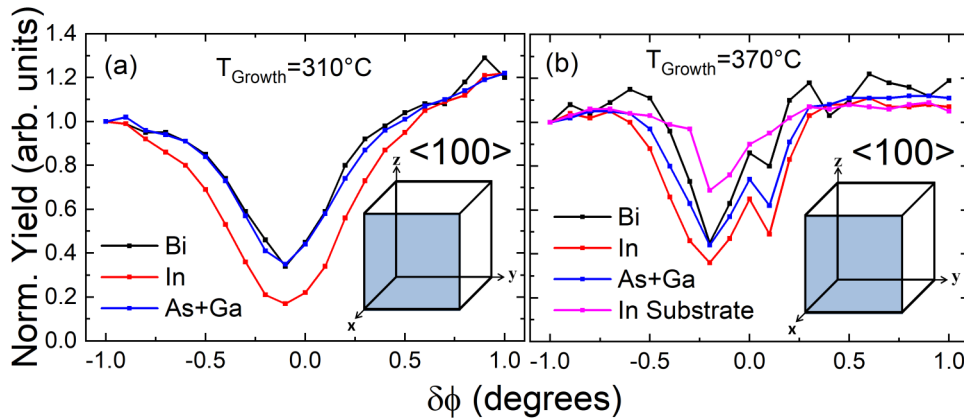


FIG. 7. Channeling RBS dips for the two InGaAs capped InGaAsBi/InP samples. (a) shows the $\langle 100 \rangle$ scan for the sample (C2) and (b) shows the $\langle 100 \rangle$ scan for the sample (C1).

therefore, highly justified to fit the bismuth peak with multiple layers, but a qualitative description of the bismuth distribution can be made by considering the bismuth peak shapes. The shape of the bismuth peak for C1, which is more peaked to lower energies, clearly suggests that there was a higher concentration of bismuth near the base of the InGaAsBi layer than at its surface, unlike C2, whose shape suggests a more homogeneous distribution; the higher bismide layer deposition temperature (370 °C vs 310 °C) appears to have caused bismuth diffusion. The bismuth distribution in UC1 may be slightly more surface peaked than UC2.

The bismuth peaks for the capped samples occur at a smaller channel number (energies) compared to the uncapped samples because of the extra energy loss of the primary beam in the cap layers. As shown in Fig. 5, the right-hand tail of the bismuth peak is more drawn out in the capped samples compared to the uncapped samples, suggesting an uneven distribution of bismuth within the InGaAsBi layer.

RBS channeling measurements

To obtain further information on substitutionality and defects in the crystal for the InGaAsBi layer, the goniometer was adjusted so that the primary ion beam was aligned along channeling

directions (crystallographic axes of the crystal). Figure 6 compares the aligned ($\langle 110 \rangle$ direction) and random RBS spectra for the uncapped samples. The lower yields for the indium, arsenic with gallium, and bismuth peaks from the aligned spectrum compared to the random spectra in Fig. 6 imply that the InGaAsBi layer has reasonable overall crystallinity. UC1 shows a higher variation in the RBS spectrum, compared to UC2. With UC2, a more defective bismide layer causes helium ion beam scattering such that the channeling in the substrate is reduced and hence closer to that of the random angle measurements.

Channeling dips could be measured by rotating the sample on the goniometer around the vertical direction, changing the incident angle of the beam to the sample. In this technique, regions that represented the signal from elements at particular depths in the sample were chosen in the RBS spectra. The intensities of the integrated signal in these regions were plotted as shown in Figs. 7 and 8 as the goniometer angle was varied by $\pm 1.5^\circ$ around the vertical axis relative to axial channeling directions. This means that the intensities in these plots have been normalized to the intensity along a planar channel direction, rather than to the random direction. Such channeling dips were collected with the beam normal to the sample for the $\langle 100 \rangle$ direction, with the goniometer at 45° to the normal for the $\langle 110 \rangle$ direction. The $\langle 111 \rangle$ direction

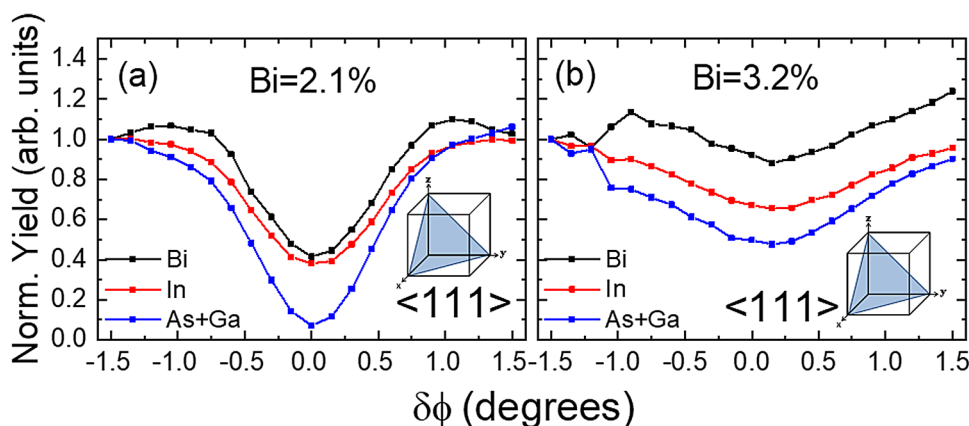


FIG. 8. Channeling RBS dips for the uncapped InGaAsBi/InP samples. (a) shows the $\langle 111 \rangle$ scan for the UC1 sample with less Bi and (b) shows the $\langle 111 \rangle$ scan for the UC2 sample with more Bi.

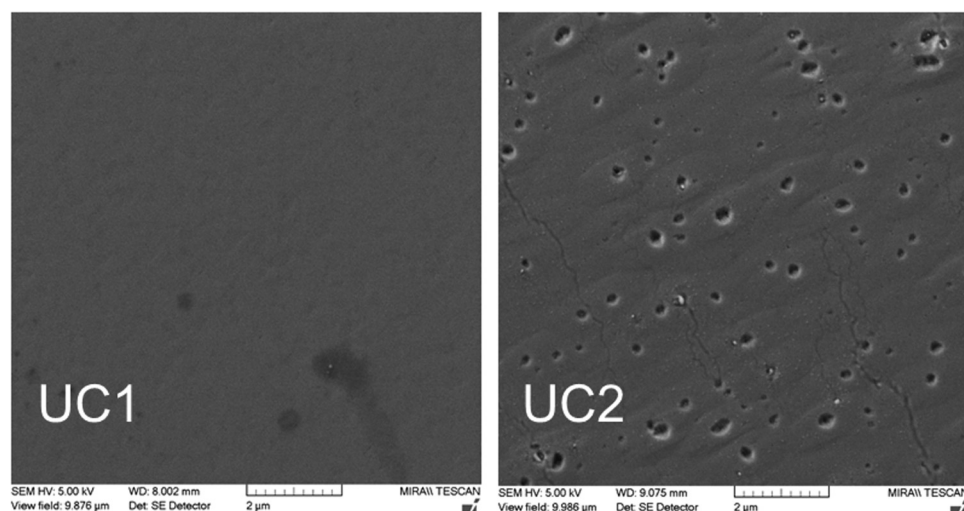


FIG. 9. SEM images of the surface of the uncapped InGaAsBi/InP samples UC1 and UC2.

is located after a rotation around the sample surface normal, with the goniometer tilted at 54.7° . Channeling dips were measured in all three directions for the uncapped samples where the regions in the RBS spectra for the surface bismide layer could easily be defined. In the capped sample spectra, assigning the regions for the bismide layer beneath the cap was more complicated, so channeling dips were only measured in the $\langle 100 \rangle$ (sample normal) direction.

The shape of the channeling dips can be instructive about the sample characteristics. Figures 7(a) and 7(b) show $\langle 100 \rangle$ channeling dips for the C2 (310°C) and C1 (370°C) samples. Figure 7(a) shows a channeling dip that is symmetric either side of the minimum with a low intensity, suggesting that there were few defects, such as interstitial atoms, present in the channels to scatter the beam. In contrast, Fig. 7(b) shows a shallower channel, indicative of crystal defects. It also suggests a possible steering effect whereby the channeling dip is interrupted by a waveform like pattern on one side,^{25,26} with all the elements in the InGaAsBi layer showing two minima. The deepest minimum corresponds to that in indium of the substrate. The second minimum, not present in the substrate, is often associated with strain^{25–27} or defects. However, as no clear strained layer was resolvable in XRD, the second minimum may be associated with stacking fault related defects as has been observed in metallic alloys^{28,29} and predicted for III-nitrides.^{30,31} Strain relaxation occurs by formation of strain relieving defects, which allows for the average lattice constant in the growth direction to be some value between that of its fully strained (pseudomorphic/tetragonal) and fully relaxed (cubic) values. However, the analysis of XRD and RBS data indicates that there may be some other factors at play. For example, antisites, where the group III or V sites have an element from the other site, as has also been seen in GaAs(Bi),^{32,33} may increase the observed lattice mismatch. We speculate that it is also possible that in InGaAsBi, bismuth gives rise to inhomogeneities leading to the formation of clusters or other localized structures in the layer similar to that observed in GaAsBi.^{20,34–36}

Figure 8 shows the channeling dips for both uncapped samples in the $\langle 111 \rangle$ direction. The channeling dips in the other

directions (not shown) are similar. The sample UC2 with the higher bismuth content has shallower channeling dips for all elements compared to UC1, indicating a poorer crystal quality or increased primary beam divergence during the measurement (caused by an amorphous surface layer). This is supported by the decreased crystalline scattering observed in XRD along with the sample having the lowest intensity PL further indicating poor crystallinity. Additionally, observations of surface roughness from the SEM images (Fig. 9) showed a nonuniform surface for UC2 with submicrometer islands and clusters or droplets. This could indicate the presence of droplets in the sample, as previously reported for InGaAsBi³⁷ and observed in GaAsBi.³⁸ Sample UC1 had a smooth surface with no visible surface inhomogeneity or defects, which supports the greater crystallinity of this sample shown by XRD and RBS.

CONCLUSIONS

In conclusion, using a combination of PL, XRD, and RBS measurements, we have investigated the properties of MBE-grown InGaAsBi layers with and without an InGaAs cap layer. Since indium and bismuth have the same effect on the lattice constant, multiple techniques are required to fully interpret the compositional and structural properties of the grown layers.

The use of multiple techniques to determine the bismuth content and structural properties of InGaAsBi samples has been shown to be important. XRD data in this work showed that the InGaAsBi layers are more homogeneous in the uncapped samples, whereas the growth of the InGaAs capped layer at higher temperature caused deterioration of the quality of the InGaAsBi layer. PL studies indicated poor optical quality of the material with no detectable PL at room temperature. Low-temperature PL exhibited multiple emission peaks, whose positions, width, and relative intensities can be used for comparative analysis of the data in line with the XRD and RBS results. Interestingly, both RBS and PL suggest some bismuth incorporation (1.2% bismuth from RBS) in the capped sample C1 grown at a higher temperature of 370°C , for

which XRD data did not demonstrate any bismuth-related feature. In this sample, the presence of strain and defects in the InGaAsBi layer was evident from the indium, gallium, arsenic, and bismuth channeling dips all exhibiting the steering effect consistent with strain and/or defects in the layer. The RBS results are in agreement with the PL observations, where a strong and broad long-wavelength emission band in the sample C1 was observed due to recombination via localized states and possible electron traps related to various defects. The second capped sample (C2) grown at a lower temperature of 310 °C exhibited much weaker localized states/traps related emission compared to C1, but showed multiple PL emission peaks at shorter wavelengths, which is associated with a variation of bismuth composition in the growth direction and suggests possibility of uneven bismuth distribution in the InGaAsBi layer due to the annealing effect during the higher temperature cap layer growth. The lower growth temperature in the sample C2 compared to C1 was advantageous in achieving a better crystalline quality and bismuth incorporation.

The two uncapped samples, UC1 and UC2, demonstrated very weak bismuth-related PL features compared to the capped samples (Fig. 3). For the uncapped samples, RBS and XRD data indicated a larger amount of bismuth in UC2 compared to UC1. The RBS analysis demonstrated evidence of a reduction of homogeneity of the InGaAsBi layer with increasing bismuth concentration. The uncapped sample (UC2), with more bismuth, showed poorer quality channeling dips with more scattering at the dip minimum due to poorer crystal quality and clustering of bismuth on the sample surface.

ACKNOWLEDGMENTS

This work was supported by the Engineering and Physical Sciences Research Council, UK (EPSRC; Project Nos. EP/H005587/1 and EP/N021037/1), which also provided a studentship for M. K. Sharpe along with a student training project at the UK National Ion Beam Centre providing beam time funded by the EPSRC (No. NS/A000059/1). The data associated with this work are available from Zenodo repository at <https://zenodo.org/record/3379098>.

REFERENCES

- ¹K. Alberi, J. Wu, W. Walukiewicz, K. M. Yu, O. D. Dubon, S. P. Watkins, C. X. Wang, X. Liu, Y.-J. Cho, and J. Furdyna, "Valence-band anticrossing in mismatched III-V semiconductor alloys," *Phys. Rev. B* **75**, 045203 (2007).
- ²J. P. Petropoulos, Y. Zhong, and J. M. O. Zide, "Optical and electrical characterization of InGaBiAs for use as a mid-infrared optoelectronic material," *Appl. Phys. Lett.* **99**, 031110 (2011).
- ³Z. Batool, K. Hild, T. J. C. Hosea, X. F. Lu, T. Tiedje, and S. J. Sweeney, "The electronic band structure of GaBiAs/GaAs layers: Influence of strain and band anti-crossing," *J. Appl. Phys.* **111**(11), 113108 (2012).
- ⁴S. J. Sweeney and S. R. Jin, "Bismide-nitride alloys: Promising for efficient light emitting devices in the near- and mid-infrared," *J. Appl. Phys.* **113**, 043110 (2013).
- ⁵I. P. Marko, Z. Batool, K. Hild, S. R. Jin, N. Hossain, T. J. C. Hosea, J. P. Petropoulos, Y. Zhong, P. B. Dongmo, J. M. O. Zide, and S. J. Sweeney, "Temperature and Bi-concentration dependence of the bandgap and spin-orbit splitting in InGaBiAs/InP semiconductors for mid-infrared applications," *Appl. Phys. Lett.* **101**(22), 221108 (2012).
- ⁶S. R. Jin and S. J. Sweeney, "InGaAsBi alloys on InP for efficient near- and mid-infrared light emitting devices," *J. Appl. Phys.* **114**, 213103 (2013).
- ⁷M. Usman, C. A. Broderick, A. Lindsay, and E. P. O'Reilly, "Tight-binding analysis of the electronic structure of dilute bismide alloys of GaP and GaAs," *Phys. Rev. B* **84**, 245202 (2011).
- ⁸Y. Gu, Y. G. Zhanga, X. Y. Chen, Y. J. Ma, S. P. Xi, B. Du, and L. Hsby, "Nearly lattice-matched short-wave infrared InGaAsBi detectors on InP," *Appl. Phys. Lett.* **108**, 032102 (2016).
- ⁹L. Wang, L. Zhang, L. Yue, D. Liang, X. Chen, Y. Li, P. Lu, J. Shao, and S. Wang, "Novel dilute bismide, epitaxy, physical properties and device application," *Crystals* **7**(3), 63 (2017).
- ¹⁰I. P. Marko, S. R. Jin, K. Hild, Z. Batool, Z. L. Bushell, P. Ludewig, W. Stolz, K. Volz, R. Butkutė, V. Pačebutas, A. Geizutis, A. Krotkus, and S. J. Sweeney, "Properties of hybrid MOVPE/MBE grown GaAsBi/GaAs based near-infrared emitting quantum well lasers," *Semicond. Sci. Technol.* **30**, 094008 (2015).
- ¹¹I. P. Marko and S. J. Sweeney, "Progress toward III-V bismide alloys for near- and midinfrared laser diodes," *IEEE J. Sel. Top. Quantum Electron.* **23**(6), 1501512 (2017).
- ¹²X. Wu, W. Pan, Z. Zhang, Y. Li, C. Cao, J. Liu, L. Zhang, Y. Song, H. Ou, and S. Wang, "1.142 μm GaAsBi/GaAs quantum well lasers grown by molecular beam epitaxy," *ACS Photonics* **4**(6), 1322–1326 (2017).
- ¹³I. P. Marko, P. Ludewig, Z. L. Bushell, S. R. Jin, K. Hild, Z. Batool, S. Reinhard, L. Nattermann, W. Stolz, K. Volz, and S. J. Sweeney, "Physical properties and optimization of GaBiAs/(Al)GaAs based near-infrared laser diodes grown by MOVPE with up to 4.4% Bi," *J. Phys. D Appl. Phys.* **47**, 345103 (2014).
- ¹⁴I. P. Marko and S. J. Sweeney, "The influence of inhomogeneities and defects on novel quantum well and quantum dot based infrared-emitting semiconductor lasers," *Semicond. Sci. Technol.* **33**(113002), 11 (2018).
- ¹⁵T. B. O. Rockett *et al.*, "Influence of growth conditions on the structural and opto-electronic quality of GaAsBi," *J. Cryst. Growth* **477**, 139–143 (2017).
- ¹⁶R. B. Lewis, M. Masnadi-Shirazi, and T. Tiedje, "Growth of high Bi concentration GaAs_{1-x}Bi_x by molecular beam epitaxy," *Appl. Phys. Lett.* **101**(8), 1–5 (2012).
- ¹⁷A. Janotti, S. H. Wei, and S. B. Zhang, "Theoretical study of the effects of isovalent co-alloying of Bi and N in GaAs," *Phys. Rev. B Condens. Matter Mater. Phys.* **65**(11), 1–5 (2002).
- ¹⁸D. F. Reyes, F. Bastiman, C. J. Hunter, D. L. Sales, A. M. Sanchez, J. P. R. David, and D. González, "Bismuth incorporation and the role of ordering in GaAsBi/GaAs structures," *Nanoscale Res. Lett.* **9**, 23 (2014).
- ¹⁹L. Gelczuk, J. Kopaczek, T. B. O. Rockett, R. D. Richards, and R. Kudrawiec, "Deep-level defects in n-type GaAsBi alloys grown by molecular beam epitaxy at low temperature and their influence on optical properties," *Sci. Rep.* **7**, 12824 (2017).
- ²⁰R. Butkutė, G. Niaura, E. Poizingytė, B. Čechavičius, A. Selskis, M. Skapas, V. Karpus, and A. Krotkus, "Bismuth quantum dots in annealed GaAsBi/AlAs quantum wells," *Nanoscale Res. Lett.* **12**, 436 (2017).
- ²¹A. Simon, C. Jeynes, R. P. Webb, R. Finnis, Z. Tatababian, P. J. Sellin, M. B. H. Breese, D. F. Fellows, R. van den Broek, and R. M. Gwilliam, "The new survey ion beam analysis facility," *Nucl. Instrum. Methods Phys. Res. Sect. B* **219**, 405–409 (2004).
- ²²M. Mayer, "Lectures given at the Workshop on Nuclear Data for Science and Technology: Materials Analysis," in *Rutherford Backscattering Spectrometry (RBS)* (Trieste, 2003), pp. 19–30.
- ²³G. Feng, K. Oe, and M. Yoshimoto, "Bismuth containing III-V quaternary alloy InGaAsBi grown by MBE," *Phys. Status Solidi A* **203**(11), 2670–2673 (2006).
- ²⁴M. Mayer, "SIMNRA, a simulation program for the analysis of NRA, RBS and ERDA," *AIP Conf. Proc.* **475**, 541 (1999).
- ²⁵S. Hashimoto *et al.*, "Steering effect at a strained NiSi₂/Si (001) interface," *Nucl. Instrum. Methods Phys. Res. Sect. B* **13**, 45–50 (1986).

- ²⁶A. Vantomme, "50 years of ion channeling in materials science," *Nucl. Instrum. Methods Phys. Res. Sect. B* **371**, 12–26 (2016).
- ²⁷K. Lorenz *et al.*, "Anomalous ion channelling in AlInN/GaN bilayers: Determination of the strain state," *Phys. Rev. Lett.* **97**, 085501 (2006).
- ²⁸C. Lu *et al.*, "Direct observation of defect range and evolution in Ion-irradiated single crystalline Ni and Ni binary alloys," *Sci. Rep.* **6**, 19994 (2016).
- ²⁹S. Zhang, K. Nordlund, F. Djurabekova, Y. Zhang, G. Velisa, and T. S. Wang, "Simulation of Rutherford backscattering spectrometry from arbitrary atom structures," *Phys. Rev. E* **94**, 043319 (2016).
- ³⁰M. A. Rana, "Ion channelling studies of defect formation in GaN and related materials," Ph.D. thesis (Department of Physics, National University of Singapore, 2005).
- ³¹A. Turos, L. Nowicki, and A. Stonert, "Ion channeling study of defects in multicomponent semiconductor compounds" (International Atomic Energy Agency (INIS), Vienna, 2002), Vol. 33, pp. 83–96, INIS No. 32, ISSN 1011-4289, Worldcat; June 2002.
- ³²J. I. Landman, "Antisite-related defects in GaAs grown at low temperatures," *Phys. Rev. Lett.* **74**(20) 4007–4010 (1995).
- ³³D. Dagnelund, J. Puustinen, M. Guina, W. M. Chen, and I. A. Buyanova, "Identification of an isolated arsenic antisite defect in GaAsBi," *Appl. Phys. Lett.* **104**, 052110 (2014).
- ³⁴J. Puustinen, M. Wu, E. Luna, A. Schramm, P. Laukkanen, M. Laitinen, T. Sajavaara, and M. Guina, "Variation of lattice constant and cluster formation in GaAsBi," *J. Appl. Phys.* **114**, 243504 (2013).
- ³⁵M. Wu, "Observation of atomic ordering of triple period A and -B type in GaAsBi," *Appl. Phys. Lett.* **105**, 041602 (2014).
- ³⁶E. Luna, "Spontaneous formation of nanostructures by surface spinodal decomposition in GaAs_{1-x}Bix epilayers," *J. Appl. Phys.* **117**, 185302 (2015).
- ³⁷Y. Zhong, P. B. Dongmo, J. P. Petropoulos, and J. M. O. Zide, "Effects of molecular beam epitaxy growth conditions on composition and optical properties of In_xGa_{1-x}Bi_yAs_{1-y}," *Appl. Phys. Lett.* **100**, 112110 (2012).
- ³⁸E. Sterzer, N. Knaub, P. Ludewig, R. Straubinger, A. Beyer, and K. Volz, "Investigation of the microstructure of metallic droplets on Ga(AsBi)/GaAs," *J. Cryst. Growth* **408**, 71–77 (2014).